Available online at www.sciencedirect.com

ScienceDirect

Ceramics International 40 (2014) 841–847

CERAMICS INTERNATIONAL

www.elsevier.com/locate/ceramint

Pt/Ga_2O_3–SiO_2 nanoparticles for efficient visible-light photocatalysis

E.S. Baeissa[a], R.M. Mohamed[a,b,*]

[a]Chemistry Department, Faculty of Science, King Abdulaziz University, P.O. Box 80203, Jeddah 21589, Saudi Arabia
[b]Advanced Materials Department, Central Metallurgical R&D Institute, CMRDI, P.O. Box 87, Helwan, Cairo, Egypt

Received 1 June 2013; received in revised form 18 June 2013; accepted 20 June 2013
Available online 10 July 2013

Abstract

Ga_2O_3–SiO_2 nanoparticles were prepared via a sol–gel method, and Pt was immobilised on the surface of Ga_2O_3–SiO_2 via a photo-assisted deposition (PAD) method. The catalytic performance of the samples was evaluated for the photocatalytic oxidation of cyanide using visible light. XRD and EDX results show that Pt is well dispersed within Ga_2O_3–SiO_2. The BET results reveal that the surface area of Ga_2O_3–SiO_2 is higher than that of the Pt/Ga_2O_3–SiO_2 samples. 0.3 wt% Pt/Ga_2O_3–SiO_2 has the highest photocatalytic activity for the degradation of cyanide. The catalyst can be reused with no loss in activity during the first 10 cycles.

Keywords: Visible photocatalyst; Pt doping; Ga_2O_3–SiO_2; Cyanide removal

1. Introduction

Environmental problems associated with hazardous wastes and toxic water pollutants have attracted much attention. Cyanides are one of the major groups of pollutants in wastewaters produced from various industries including metal cleaning, plating, electroplating, metal processing, automobile parts manufacturing, steel tempering, mining, photography, pharmaceutical manufacturing, coal coking, ore leaching, and plastics manufacturing. Among the various physical, chemical and biological techniques for treatment of wastewaters, photocatalysis is considered to be cost-effective for water remediation [1–3]. Advanced oxidation processes (AOPs), such as heterogeneous photocatalysis, have gained a great deal of attention. TiO_2 is the most popular material for these processes due to its higher photocatalytic activity, good photostability, non-toxicity, and low price. However, the large band gap of TiO_2, which is 3.2 eV, has proven to be a major drawback because wavelengths below 400 nm are necessary for excitation limiting the efficiency of solar light sources. Therefore, modification of the TiO_2 band gap would be useful for improving the optical properties of this material. In the last few decades, doping with metals and nonmetals has been successfully utilised to shift the optical response of the catalytically active TiO_2 from the UV to the visible light region. Zeolite [4,5], graphene [6], Eu [7], Bi [8], Ni [9], Pt [10], Au [11], Ag [12–15], rare earth dopants [16,17], Co, Cr and Ag [18,19] have been used to extend the photoresponse range of the TiO_2 matrix. Gallium oxide was reported as a water splitting photocatalyst for the generation of hydrogen gas. β-Ga_2O_3 is a wide band gap semiconductor that has versatile applications in optoelectronic devices, high temperature electronic devices and high temperature stable gas sensors [20–22]. Recently, it was reported that nanophases of gallium oxide could be used as an efficient photocatalyst for the oxidative degradation of organic effluents [23–29]. The main drawback associated with the β-Ga_2O_3 semiconductor photocatalyst is its low surface area and absorption in the UV region. Therefore, the main goal for researchers is to increase the surface area of β-Ga_2O_3 by employing an inert support (i.e., SiO_2 and Al_2O_3) and to convert the absorption from UV to visible light via metal doping.

To the best of our knowledge, there are no reports of degradation of cyanide in an aqueous solution using gallium oxide. The present study aims to synthesise and characterise Pt/β-Ga_2O_3–SiO_2 as well as evaluate its photocatalytic activity

*Corresponding author at: Chemistry Department, Faculty of Science, King Abdulaziz University, P.O. Box 80203, Jeddah 21589, Saudi Arabia. Tel.: +966 540715648; fax: +966 2 6952292.
E-mail address: mhmdouf@gmail.com (R.M. Mohamed).

0272-8842/$ - see front matter © 2013 Elsevier Ltd and Techna Group S.r.l. All rights reserved.
http://dx.doi.org/10.1016/j.ceramint.2013.06.077

for the oxidative degradation of cyanide in aqueous phase under visible light.

2. Experimental

The reagents employed include the following chemicals: tetraethylorthosilicate $Si(OC_2H_5)_4$ (TEOS), purity 98%, Acros; gallium isoperoxide $Ga(OC_3H_7)_3$, (GP), Aldrich; ethanol C_2H_5OH, Absolute, Aldrich; nitric acid HNO_3, Aldrich; and chloroplatinic acid H_2PtCl_6, Sigma-Aldrich.

0.2 Ga_2O_3: 1 SiO_2 nanoparticles were prepared via a sol–gel method. A total of 20 ml TEOS was mixed with ethyl alcohol (C_2H_5OH), ultra pure water (H_2O) and nitric acid (HNO_3) as the catalyst under magnetic stirring for 60 min. Then, a calculated amount of $Ga(OC_3H_7)_3$ was slowly added to the previous mixture with continuous stirring for 60 min. The prepared sol was left to stand in air to form the gel. The gel sample was calcined at 550 °C for 5 h in air to obtain the Ga_2O_3–SiO_2 xerogel.

Pt/Ga_2O_3–SiO_2 catalysts (0.1, 0.2, 0.3 and 0.4 wt% of Pt metal) were synthesised using a photo-assisted deposition (PAD) route. First, Pt metal was deposited on Ga_2O_3–SiO_2 from an aqueous solution of H_2PtCl_6 under UV light irradiation. Then, the samples were dried at 378 K followed by H_2 reduction (20 ml min^{-1}) at 400 °C for an additional 2 h.

X-ray diffraction (XRD) analysis was performed at room temperature using a Bruker axis D8 using Cu Kα radiation (λ=1.540 Å) over a 2θ collection range of 10–80° with a step scan of 0.020 and a step time of 0.4 s. The specific surface area was calculated from N_2 adsorption measurements using a Nova 2000 series Chromatech apparatus. Prior to the measurements, all of the samples were treated under vacuum at 200 °C for 2 h. The band gap of the samples was determined by UV–vis diffuse reflectance spectra (UV–vis–DRS) in air at room temperature in the wavelength range of 200–800 nm using a UV/vis/NIR spectrophotometer (V-570, JASCO, Japan). Transmission electron microscopy (TEM) was performed with a JEOL-JEM-1230 microscope. The samples were prepared by suspending a small amount of each sample in ethanol followed by ultrasonication for 30 min. Then, a small amount of this solution was placed onto a carbon coated copper grid and dried before loading the sample in the TEM. Photoluminescence (Pl) emission spectra were recorded with a fluorescence spectrophotometer Shimadzu RF-5301. The application of the synthesised nanocomposite for the photodegradation of cyanide was investigated under visible light. The experiments were performed using a horizontal cylinder annular batch reactor. The photocatalyst was irradiated with a blue fluorescent lamp (150 W, maximum energy at 450 nm) doubly covered with a UV cut filter. The intensity data of the UV light was less than the detection limit (0.1 mW/cm^2) of a UV radiometer. In a typical experiment, 0.2 g of catalyst was suspended in a 300 ml solution of 100 mg/l potassium cyanide (KCN, pH=10.5 to avoid the evolution of HCN gas), which was adjusted using an ammonia solution. The reaction was performed isothermally at 25 °C, and samples of the reaction mixture were taken at different intervals during the 1 h reaction. The $CN^-_{(aq)}$ concentration in the samples was estimated by volumetric titration with $AgNO_3$, and potassium iodide was employed to determine the titration endpoint [30]. The removal efficiency of $CN^-_{(aq)}$ has been measured by applying the following equation:

$$\%\ \text{removal efficiency} = (\text{Co} - C)/\text{Co} \times 100$$

where Co is the initial concentration of uncomplexed $CN^-_{(aq)}$ in solution and C is the concentration of unoxidized $CN^-_{(aq)}$ in solution.

The adsorption of the catalysts is determined in the same manner as the photocatalytic activity measurements with the only difference being that the adsorption process was conducted without light irradiation. The results reveal that approximately 3% of cyanide was adsorbed by the Ga_2O_3–SiO_2 and Pt/Ga_2O_3–SiO_2 samples after 1 h in dark. Therefore, the adsorption of cyanide on the catalyst is very small, and the process that is occurring is photocatalysis.

The repeated experiments for the photodegradation of cyanide were performed to evaluate the photochemical stability of the catalyst and were performed using the same procedure employed for the photocatalytic activity measurements except that the catalyst was reused many times.

3. Results and discussion

3.1. Structural, morphological and compositional characterisations

The XRD patterns of each parent Ga_2O_3–SiO_2 and Pt/Ga_2O_3–SiO_2 nanoparticle prepared via the PAD method are displayed in Fig. 1. The structural characteristics of Ga_2O_3–SiO_2 and Pt/Ga_2O_3–SiO_2 are consistent with a monoclinic β-Ga_2O_3 structure, which is in good agreement with the reported values of β-Ga_2O_3 (JCPDS: 41-1103). This result indicated that the β-Ga_2O_3 structure remained after the application of the photo-assisted deposition (PAD) method. However, no diffraction peaks associated with Pt in the patterns of the Pt/Ga_2O_3–SiO_2

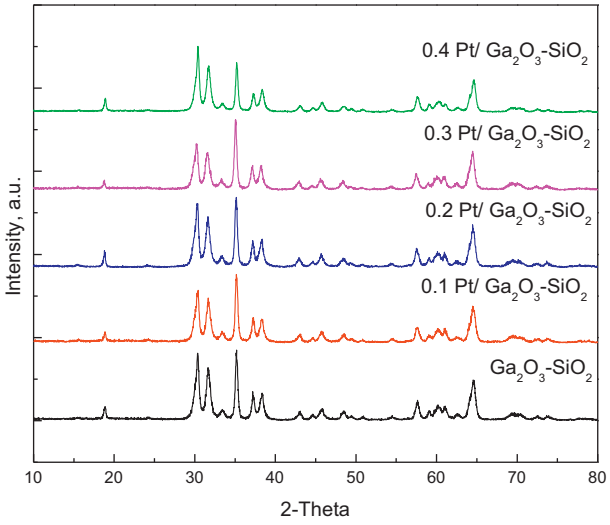

Fig. 1. XRD pattern of the β-Ga_2O_3–SiO_2 and Pt/β-Ga_2O–SiO_2 nanoparticles.

samples were observed because the amount of Pt was less than the detection limit. In addition, the data may imply that Pt is well dispersed within the Ga_2O_3–SiO_2 phase.

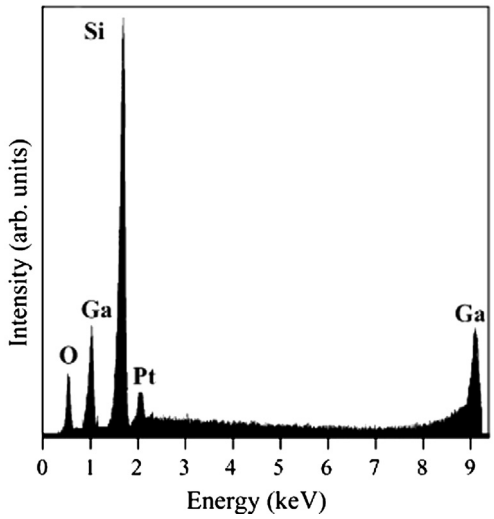

Fig. 2. EDAX analysis results for 0.3 Pt/β-Ga_2O–SiO_2.

The results of the EDAX analysis, which only identifies the surface elements on the sample, are shown in Fig. 2. A signal for Pt was detected on the surface of the catalyst, which confirmed the successful loading of Pt ions via the PAD method.

The TEM images of the Pt/Ga_2O_3–SiO_2 nanoparticles prepared using the PAD method are shown in Fig. 3. The results reveal that the Pt ions were dispersed on the surface of the catalyst, and the diameter of the Pt ion increased as the wt% of Pt increased. It is clear that the homogeneity of Pt increased as the amount of Pt ions increased to 0.3 wt%. In addition, at higher concentration of Pt ions (i.e., 0.4 wt%), the homogeneity of Pt decreased. This observation indicated that there was an optimum value for the deposition of Pt ions.

3.2. Surface area analysis

Specific surface area (S_{BET}) of the parent Ga_2O_3–SiO_2 and Pt/Ga_2O_3–SiO_2 nanoparticles was determined. The S_{BET} values were 400, 393, 360, 349 and 341 m^2/g for Ga_2O_3–SiO_2, 0.1 Pt/Ga_2O_3–SiO_2, 0.2 Pt/Ga_2O_3–SiO_2, 0.3 Pt/Ga_2O_3–SiO_2 and 0.4

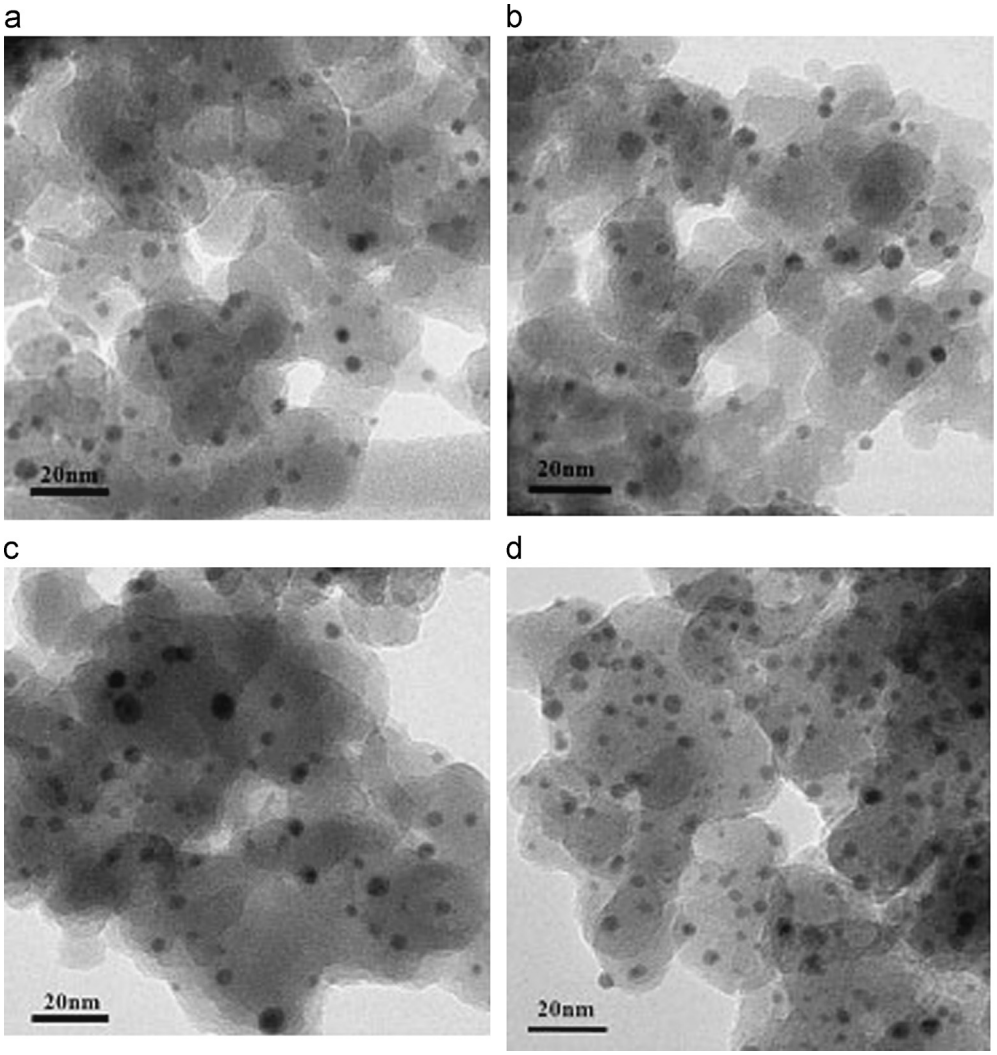

Fig. 3. TEM images of the Pt/Ga_2O_3–SiO_2 nanoparticles where the wt% of Pt is 0.1 (a), 0.2 (b), 0.3 (c) and 0.4 (d).

Table 1
Texture parameters of the Ga_2O_3–SiO_2 and Pt/Ga_2O_3–SiO_2 nanoparticles.

Sample	S_{BET}[a] (m^2/g)	S_t[b] (m^2/g)	S_{micro}[c] (cm^2/g)	S_{meso} (cm^2/g)	S_{ext}[d] (cm^2/g)	V_p[e] (cm^3/g)	V_{micro}[f] (cm^3/g)	V_{meso}[g] (cm^3/g)	r[h] (Å)
Ga_2O_3–SiO_2	400	417	323	264	77	0.890	0.080	0.810	36.00
0.1 Pt/Ga_2O_3–SiO_2	393	410	325	259	68	0.790	0.070	0.730	38.00
0.2 Pt/Ga_2O_3–SiO_2	360	375	300	238	60	0.720	0.060	0.660	39.00
0.3 Pt/Ga_2O_3–SiO_2	349	364	299	230	58	0.700	0.055	0.648	40.00
0.4 Pt/Ga_2O_3–SiO_2	341	355	295	225	46	0.690	0.050	0.640	41.00

Note:
[a](S_{BET})—BET-surface area.
[b](S_t)—surface area derived from the V_{l-t} plots.
[c](S_{micro})—surface area of micropores.
[d](S_{ext})—external surface area.
[e](V_p)—total pore volume.
[f](V_{micro})—pore volume of micropores.
[g](V_{meso})—pore volume of mesopores.
[h](r)—mean pore radius.

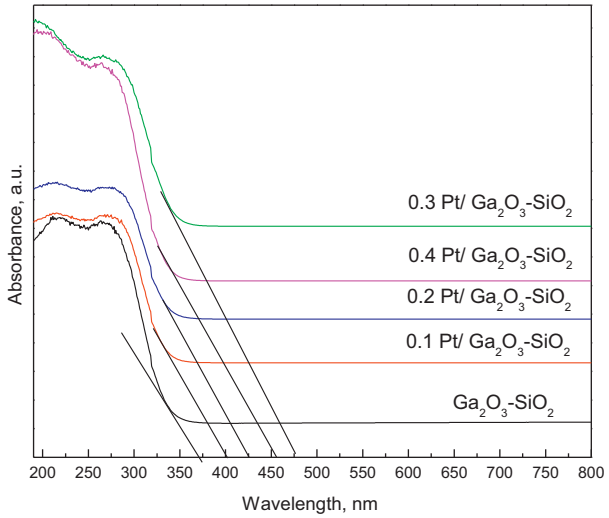

Fig. 4. Diffuse reflectance UV–vis absorption spectra of the β-Ga_2O_3–SiO_2 and Pt/β-Ga_2O–SiO_2 nanoparticles.

Pt/Ga_2O_3–SiO_2, respectively. The surface area parameters and the data calculated from the *t*-plot are provided in Table 1. In addition, the total pore volume of Ga_2O_3–SiO_2 is higher than that of the Pt/Ga_2O_3–SiO_2 samples due to blocking of some of the pore by deposition of Pt metal. In general, the values of S_{BET} and S_t are similar for most of the samples indicating the presence of mesopores.

3.3. Optical characterisation

The UV–vis diffuse reflectance spectra of the Ga_2O_3–SiO_2 and Pt/Ga_2O_3–SiO_2 nanoparticles are displayed in Fig. 4. The loading of Pt ions into Ga_2O_3–SiO_2 caused a red shift toward higher wavelength from 383 to 448 nm for different loadings of Pt compared to Ga_2O_3–SiO_2 which had a wavelength of approximately 357 nm. The direct band gap energy for Ga_2O_3–SiO_2 and Pt/Ga_2O_3–SiO_2 was calculated from their reflection spectra based on a method suggested by Kumar et al. [31]. The band gap energies were calculated according to the following equation:

$$E_g = 1239.8/\lambda$$

where E_g is the band gap (eV) and λ is the wavelength of the absorption edges in the spectrum (nm). The results are shown in Table 2. The energy gap decreased as the content of Pt ions increased to 0.3 wt%. In addition, at a higher concentration of Pt ions (i.e., 0.4 wt%), the band gap increased again. This observation indicated that there was an optimum value for doping with Pt ions.

Table 2
Band gap energy of the Ga_2O_3–SiO_2 and Pt/Ga_2O_3–SiO_2 nanoparticles.

Sample	**Band gap energy, eV**
Ga_2O_3–SiO_2	3.47
0.1 Pt/Ga_2O_3–SiO_2	3.24
0.2 Pt/Ga_2O_3–SiO_2	3.00
0.3 Pt/Ga_2O_3–SiO_2	2.77
0.4 Pt/Ga_2O_3–SiO_2	2.92

Photoluminescence (Pl) emission spectra have been used to study the transfer of photogenerated electrons and holes and to understand the separation and recombination of photogenerated charge carriers. To investigate the photoelectric properties of the prepared samples, the Pl spectra were recorded for the different samples excited at 265 nm at room temperature, as shown in Fig. 5. The position of the emission of Ga_2O_3–SiO_2 is different compared to the Pt/Ga_2O_3–SiO_2 samples, and the Pl intensity substantially decreased as the content of Pt increased to 0.3 wt%. At a higher concentration of Pt ions (i.e., 0.4 wt%), the Pl intensity increased again, which is in agreement with the UV–vis results. Pt acts as a trapping site to capture photogenerated electrons from the conduction band separating the photogenerated electron–hole pairs. In general, the incorporation of noble metal nanoparticles into semiconductor-based catalysts might enhance the light absorption of a catalyst in the visible light region resulting in a shift of the

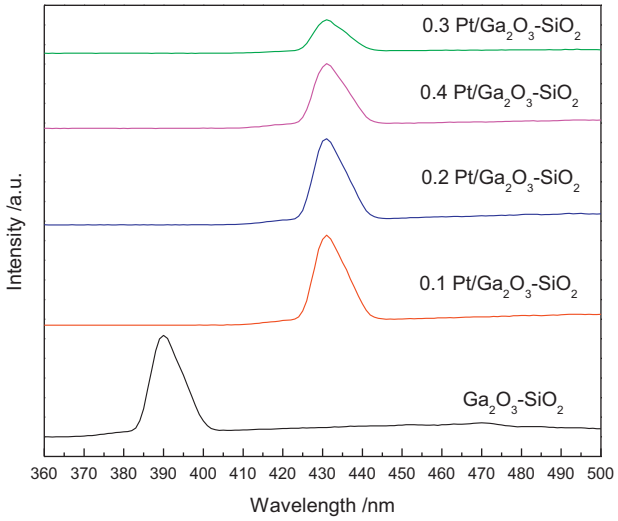

Fig. 5. Pl spectra of the β-Ga_2O_3–SiO_2 and Pt/β-Ga_2O–SiO_2 nanoparticles.

absorption edge toward longer wavelengths. This shift indicates a decrease in the band gap energy allowing for more photogenerated electrons and holes that can participate in photocatalytic reactions. When Pt acts as a noble metal, it appears to modify the interface of Ga_2O_3–SiO_2 altering the mechanism that photogenerated charge carriers undergo recombination or surface reactions. This change would force the Ga_2O_3–SiO_2 mixed oxide to be activated in the visible region. The shift in the emission position could be attributed to the charge transfer between the Pt generated band and the conduction band of Ga_2O_3–SiO_2 as a semiconductor.

3.4. Photocatalytic activities

In general, the process of photocatalysis by semiconductors begins with the direct absorption of supra-band gap photons and the generation of electron–hole pairs in the semiconductor particles. This step is followed by diffusion of the charge carriers to the surface of the particle. The photocatalytic reactions can be listed as follows:

$$Ga_2O_3 + h\nu \rightarrow e^-_{CB} + h^+_{VB}$$
$$e^-_{CB}(Pt) \rightarrow e^-_{tr}(Pt)$$
$$e^-_{tr} + O_2(ads) \rightarrow O_2^-$$
$$2e^-_{tr} + 2H^+ + O_2 \rightarrow H_2O_2$$
$$H_2O_2 + e^-_{tr} \rightarrow HO^- + HO^\bullet$$
$$h^+_{VB} + H_2O \rightarrow H^+ + HO^\bullet$$
$$2CN^- + 4HO^\bullet \rightarrow N_2 + 2CO_2 + 2H_2$$

The photocatalytic activity is believed to be associated with highly reactive peroxide (O_2^-) and hydroxyl radical ($HO^\bullet$) species generated by electrons and holes on the surface with water. If surface defect states exist, they may be able to trap the electron or hole preventing the recombination and increasing the rate of the oxidation–reduction reactions. In our case, Pt acts as an electron trap, and the rate of photocatalytic activity increased. The photocatalytic activity is known to be dependent on the crystallinity, surface area and morphology, and it may be improved by slowing the recombination of photogenerated electron–hole pairs, which shifts the excitation wavelength to a lower energy range and increases the amount of surface-adsorbed reactant species.

Fig. 6 shows the photocatalytic degradation of a cyanide solution with the role of Ga_2O_3–SiO_2 catalyst with different wt % of Pt under visible light. The experiment was performed under the following conditions: pH of the solution was 10.5 pH, 100 ppm of KCN, 300 ml of KCN and 0.20 g of catalyst. The results indicate that Ga_2O_3–SiO_2 and 0.1 Pt/Ga_2O_3–SiO_2 exhibit very little photocatalytic activity under visible light due to their absorbance in the UV region. In addition, an increase in the wt% of Pt from 0.2 to 0.3 leads to a high cyanide removal efficiency from 55% to 100%, respectively. However, a further increase in the wt% of Pt above 0.3 wt% decreased the cyanide removal efficiency to 88%.

The reaction order with respect to cyanide was determined by plotting the reaction time as a function of log[cyanide] according to the following equation for Ga2O3–SiO_2 and Pt/Ga_2O_3–SiO_2 samples:

$$\log[C]_t = -kt + \log[C]_o$$

where $[C]_0$ and $[C]_t$ represent the concentration of the substrate in solution at time zero and the time of illumination, respectively, and k represents the apparent rate constant (min^{-1}).

The apparent rate constants are summarised in Table 3. The results show that the reaction followed first order kinetics with respect to cyanide, and the rate constants were determined to be 10×10^{-4} to $160 \times 10^{-4}\,min^{-1}$. The first order rate equation for cyanide is given by $R = k$[cyanide].

Fig. 7 shows the photocatalytic degradation of the cyanide solution with the role of Ga_2O_3–SiO_2 catalyst with different catalyst loadings under visible light, and the experiment was performed under the following conditions: pH of the solution was 10.5, 100 ppm of KCN, 300 ml of KCN and 0.3 wt% of Pt/Ga_2O_3–SiO_2. The results indicate that an increase in the catalyst loading from 0.1 to 0.20 g resulted in an increase in the cyanide removal efficiency from 94% to 100%, respectively, after reaction time of 60 min. However, a further increase in the catalyst loading from 0.2 to 0.3 g decreased the reaction time from 60 to 45 min. For a catalyst loading greater than 0.3 g, no significant effect on cyanide removal efficiency and reaction time was observed. Therefore, the optimum condition for the catalyst loading was 0.30 g.

The reaction order with respect to cyanide was determined by plotting the reaction time as a function of log[cyanide] according to the following equation for the samples with different catalyst loadings:

$$\log[C]_t = -kt + \log[C]_o$$

where $[C]_0$ and $[C]_t$ represent the concentration of the substrate in solution at time zero and the time of illumination, respectively, and k represents the apparent rate constant (min^{-1}).

The apparent rate constants are summarised in Table 4. The results show that the reaction followed first order kinetics

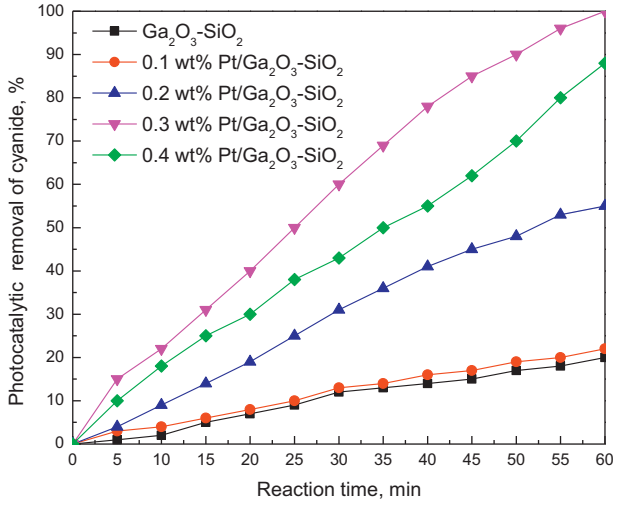

Fig. 6. Effect of wt% of Pt on the photocatalytic activity of Ga_2O_3–SiO_2 for cyanide removal.

Table 3
Rate constant of cyanide with the Ga_2O_3–SiO_2 and Pt/Ga_2O_3–SiO_2 samples.

Sample	$k \times 10^{-4}$, min^{-1}
Ga_2O_3–SiO_2	10
0.1% Pt/Ga_2O_3–SiO_2	10
0.2% Pt/Ga_2O_3–SiO_2	50
0.3% Pt/Ga_2O_3–SiO_2	160
0.4% Pt/Ga_2O_3–SiO_2	90

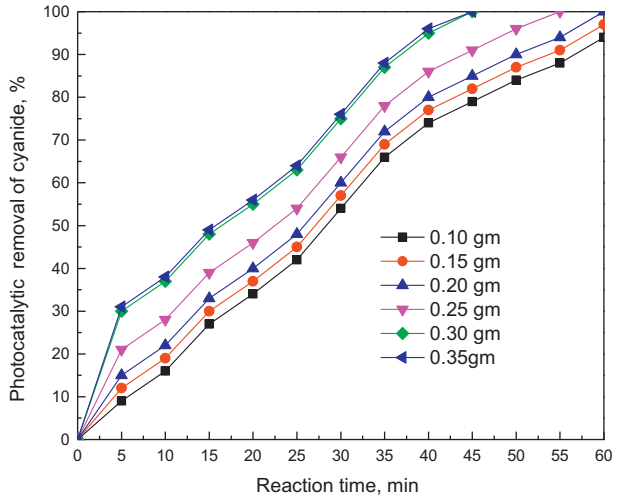

Fig. 7. Effect of loading of 0.3 wt% Pt/Ga_2O_3–SiO_2 on the photocatalytic removal of cyanide.

with respect to cyanide, and the rate constants were determined to be 120×10^{-4} to 240×10^{-4} min^{-1}. The first order rate equation for cyanide is given by $R = k$[cyanide].

The repeated experiments for the photodegradation of cyanide were performed on the 0.3 wt% Pt/Ga_2O_3–SiO_2 sample to evaluate the photochemical stability of the catalyst, and the results are shown in Fig. 8. After each photocatalytic reaction,

Table 4
Rate constant for cyanide with different loadings of the 0.3 wt% Pt/Ga_2O_3–SiO_2 sample.

Loading of 0.3 wt% Pt/Ga_2O_3–SiO_2, g	$k \times 10^{-4}$, min^{-1}.
0.10	120
0.15	130
0.2	160
0.25	170
0.3	240
0.35	250

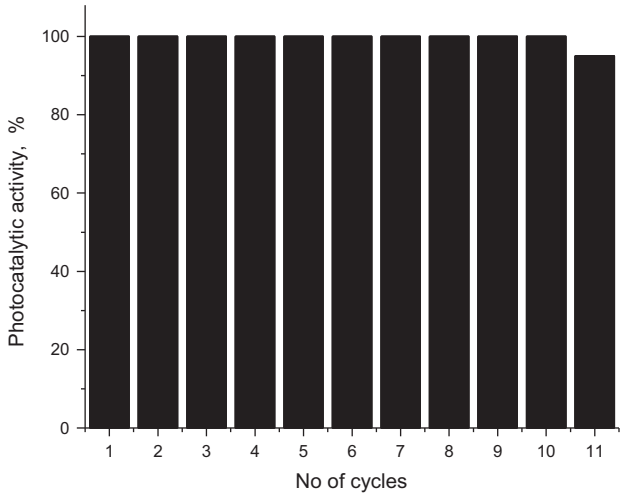

Fig. 8. Photochemical stability of 0.3 wt% Pt/Ga_2O_3–SiO_2.

the sample was retained for reuse without further treatment. The photocatalyst was utilised to repeatedly photodegrade cyanide under irradiation with visible light. The photocatalytic performance was 100% during the first 10 cycles. The photocatalytic activity of the recycled photocatalyst decreased by a ratio of 5% after 10 cycles. Therefore, the separation of the photocatalyst was effective, and the consistent photocatalytic activity of the Pt/Ga_2O_3–SiO_2 is promising for future applications.

4. Conclusions

In summary, the Pt/Ga_2O_3–SiO_2 photocatalyst was successfully synthesised, and it was proven to be a promising catalyst due to its high removal efficiency of the pollutant under visible light. The red shift phenomenon was found to depend on the wt% of Pt doped on Ga_2O_3–SiO_2, which has been observed in the UV–vis spectra of the Ga_2O_3–SiO_2 and Pt/Ga_2O_3–SiO_2 samples. Photocatalytic measurements during the photocatalytic degradation of the cyanide solution showed that the Pt/Ga_2O_3–SiO_2 nanoparticles with 0.3 wt% of Pt exhibited the highest catalytic activity as well as efficient photocatalytic properties in water purification. Therefore, this catalyst may find potential application in related fields. In addition, the catalyst was reused with no loss of activity during the first 10

cycles. The degradation efficiency of cyanide remained high (i.e., approximately 95%) after the photocatalyst was used 11 times.

Acknowledgement

This paper was funded by the Deanship of Scientific Research (DSR), King Abdulaziz University, Jeddah, under Grant no. (247-002-D1433). Therefore, the authors acknowledge the DSR technical and financial support.

References

[1] N.R. Khalid, E. Ahmed, Z. Hong, M. Ahmad, Y. Zhang, S. Khalid, Photocatalysis, Ceramics International 39 (2013) 7107–7113.
[2] P. Wei, J. Liu, Z. Li, Effect of Pt loading and calcination temperature on the photocatalytic hydrogen production activity of TiO_2 microspheres, Ceramics International 39 (2013) 5387–5391.
[3] H. Matsui, N. Ohkura, S. Karuppuchamy, M. Yoshihara, The effect of surface area on the photo-catalytic behavior of ZrO_2/carbon clusters composite materials, Ceramics International 39 (2013) 5827–5831.
[4] R.M. Mohamed, E.S. Baeissa, Mordenite encapsulated with Pt-TiO_2: characterization and applications for photocatalytic degradation of direct blue dye, Journal of Alloys and Compounds 558 (2013) 68–72.
[5] R.M. Mohamed, M.M. Mohamed, Copper(II) phthalocyanines immobilized on alumina and encapsulated inside zeolite X and their applications in photocatalytic degradation of cyanide: a comparative study, Applied Catalysis A 340 (2008) 16–24.
[6] R.M. Mohamed, UV-assisted photocatalytic synthesis of TiO_2-reduced graphene oxide with enhanced photocatalytic activity in decomposition of Sarin in gas phase, Desalination and Water Treatment 50 (2012) 147–156.
[7] M. Vranješ, J. Kuljanin-Jakovljević, T. Radetić, M. Stoiljković, M. Mitrić, Z.V. Šaponjić, J. Nedeljković, Structure and luminescence properties of Eu^{3+} doped TiO_2 nanocrystals and prolate nanospheroids synthesized by the hydrothermal processing, Ceramics International 38 (2012) 5629–5636.
[8] M.N. An'amt, S. Radiman, N.M. Huang, M.A. Yarmo, N.P. Ariyanto, H.N. Lim, M.R. Muhamad, Sol–gel hydrothermal synthesis of bismuth–TiO_2 nanocubes for dye-sensitized solar cell, Ceramics International 36 (2010) 2215–2220.
[9] R.M. Mohamed, E.S. Aazam, H_2 production with low CO selectivity from photocatalytic reforming of glucose on Ni/TiO_2–SiO_2: synthesis and nanostructure characterization, Chinese Journal of Catalysis 33 (2012) 247–253.
[10] R.M. Mohamed, E.S. Aazam, Preparation and characterization of platinum doped porous titania nanoparticles for photocatalytic oxidation of carbon monoxide, Journal of Alloys and Compounds 509 (2011) 10132–11038.
[11] R.M. Mohamed, E.S. Aazam, Characterization and catalytic properties of nano-sized au metal catalyst on titanium containing high mesoporous silica (Ti-HMS) synthesized by photo-assisted deposition and impregnation methods, International Journal of Photoenergy (2011) 7 Article ID 137328.
[12] B. Aysin, A. Ozturk, J. Park, Silver-loaded TiO_2 powders prepared through mechanical ball milling, Ceramics International 39 (2013) 7119–7126.
[13] S. Ramya, S.D. Ruth Nithila, R.P. George, D.Nanda Gopala Krishna, C. Thinaharan, U. Kamachi Mudali, Antibacterial studies on Eu–Ag codoped TiO_2 surfaces, Ceramics International 39 (2013) 1695–1705.
[14] R.M. Mohamed, I.A. Mkhalid, Characterization characterization and catalytic properties of nano-sized Ag metal catalyst on TiO_2–SiO_2 synthesized by photo-assisted deposition (PAD) and impregnation methods, Journal of Alloys and Compounds 501 (2010) 301–306.
[15] R.M. Mohamed, I.A. Mkhalid, The effect of rare earth dopants on the structure, surface texture and photocatalytic properties of TiO_2–SiO_2 prepared by sol–gel method, Journal of Alloys and Compounds 501 (2010) 143–147.
[17] R.M. Mohamed, L.D. Mickinny, M.W. Sigmund, Enhanced nanocatalysts, Materials Science and Engineering: R 73 (2012) 1–13.
[18] Z.M. El-Bahy, A.A. Ismail, R.M. Mohamed, Enhancement of the photocatalytic properties of titania nanoparticles by doping with rare earth ions, Journal of Hazardous Materials 166 (2009) 138–143.
[19] R.M. Mohamed, K. Mori, H. Yamashita, Effect of Ag, Co and Cr deposit on the photocatalytic activity of titania–silica for the removal of 2-propanol in water, International Journal of Nanoparticles 2 (2009) 533–542.
[20] L. Jun, Y. Min, L. Cuikun, L. Xiaoming, Multiform oxide optical materials via the versatile pechini-type sol–gel process: synthesis and characteristics, Journal of Physical Chemistry C 111 (2007) 5835–5845.
[21] R.Z. Dai, W.Z. Pan, L.Z. Wang, Novel nanostructures of functional oxides synthesized by thermal evaporation, Advanced Functional Materials 13 (2003) 9–24.
[22] H. Seshadri, P.K. Sinha, Photocatalytic performance of combustion synthesized β-Ga_2O_3 for the degradation of tri-*n*-butyl phosphate in aqueous solution, Sensors and Actuators B 93 (2003) 431–434.
[23] H. Yidong, Z. Jinshui, D. Zhengxin, W. Ling, Synthesis, characterization and photocatalytic activity of β-Ga_2O_3 nanostructures, Powder Technology 203 (3) (2010) 440–446.
[24] H. Yidong, W. Ling, W. Xinchen, D. Zhengxin, L. Zhaohui, F. Xianzhi, Efficient decomposition of benzene over a β-Ga_2O_3 photocatalyst under ambient conditions, Environmental Science and Technology 40 (2006) 5799–5803.
[25] H. Yidong, W. Ling, W. Xinchen, D. Zhengxin, L. Zhaohui, F. Xianzhi, Photocatalytic performance of α-, β-, and γ-Ga_2O_3 for the destruction of volatile aromatic pollutants in air, Journal of Catalysis 250 (2007) 12–18.
[26] K. Girija, S. Thirumalairajan, Astam K. Patra, D. Mangalaraj, N. Ponpandian, C. Viswanathan, Enhanced photocatalytic performance of novel self-assembled floral β-Ga_2O_3 nanorods, Current Applied Physics 13 (2013) 652–658.
[27] Z. Baoxiu, L. Mou, Z. Li, Photocatalytic degradation of perfluorooctanoic acid with β-Ga_2O_3 in anoxic aqueous solution, Journal of Environmental Sciences 24 (2012) 774–780.
[28] Z. Weirong, Y. Yong, H. Rui, L. Feifei, W. Yan, T. Min, T. Jing, R. Daqing, Z. Dongye, Synthesis of mesoporous β-Ga_2O_3 nanorods using PEG as template: preparation, characterization and photocatalytic properties, Journal of Hazardous Materials 192 (2011) 1548–1554.
[29] H. Yidong, Z. Jinshui, D. Zhengxin, W. Ling, Synthesis, characterization and photocatalytic activity of β-Ga_2O_3 nanostructures, Powder Technology 203 (2010) 440–446.
[30] I.A. Vogel, Quantitative Inorganic Analysis, Longmans, London, 1978.
[31] V. Kumar, K.S. Sharma, P.T. Sharma, V. Singh, Band gap determination in thick films from reflectance measurements, Optical Materials 12 (1999) 115–119.